Eur. Phys. J. C (2024) 84:485
https://doi.org/10.1140/epjc/s10052-024-12769-8

THE EUROPEAN PHYSICAL JOURNAL C

Regular Article -Theoretical Physics

Gravitational wave effects and phenomenology of a two-component dark matter model

Mojtaba Hosseini[1,a], **Seyed Yaser Ayazi**[1,b], **Ahmad Mohamadnejad**[2,c]

[1] Physics Department, Semnan University, P.O. Box. 35131-19111, Semnan, Iran
[2] Department of Physics, Lorestan University, Khorramabad, Iran

Received: 30 November 2023 / Accepted: 5 April 2024 / Published online: 10 May 2024

Abstract We study an extension of the Standard Model (SM) which could have two candidates for dark matter (DM) including a Dirac fermion and a vector dark matter (VDM) under a new $U(1)$ gauge group in the hidden sector. The model is classically scale-invariant and the electroweak symmetry breaks because of loop effects. We investigate the parameter space allowed by current experimental constraints and phenomenological bounds. We probe the parameter space of the model in the mass range $1 < M_V < 5000$ GeV and $1 < M_\psi < 5000$ GeV. It has been shown that there are many points in this mass range that are in agreement with all phenomenological constraints. The electroweak phase transition has been discussed and it has been shown that there is region in the parameter space of the model consistent with DM relic density and direct detection constraints that, at the same time, can lead to first-order electroweak phase transition. The gravitational waves produced during the phase transition could be probed by future space-based interferometers such as LISA and BBO.

1 Introduction

The Standard Model (SM) has been the most effective way to describe the functioning of the world around us, but is incomplete because of challenges like matter–antimatter asymmetry, hierarchy problem, and dark matter (DM). DM is estimated to make up approximately 27% of our universe, as indicated by a lot of astrophysical and cosmological evidence [1]. One of the main goals of particle physicists is to predict and find a particle that can satisfy the properties of DM, which can be a window to physics beyond the standard model (BSM).

Weakly interacting massive particles (WIMPs) are the most popular candidate for DM, with the freeze-out scenario being the most popular choice [2]. The WIMP paradigm is essential background for almost any discussion of particle DM and the triple coincidence of motivations from particle theory, particle experiment, and cosmology is known as the WIMP miracle. However, no trace of DM has so far been found in direct detection experiments. Due to strong constraints on direct detection experiments in one-component DM models, multi-component DM models seem more appropriate in some ways [3–53].

In the SM, electroweak phase transition is of the second order [54,55] and does not generate the gravitational wave (GW) signal (for a recent review see [56]). A first-order phase transition can be caused by certain extensions of the SM and the DM candidate, leading to the creation of GWs [57–85]. In the early universe, when two local minima of free energy (potential) co-exist for some range of temperatures (critical temperature), strongly first-order electroweak phase transition can take place. After that, the relevant scalar fields can quantum-mechanically tunnel into the new phase and through the nucleation of bubbles and collide with each other to cause a significant background of GWs [86–90].The discovery of GWs resulting from the first-order phase transition can be the consequence of physics BSM, which can be a supplement to ground experiments like those conducted using the Large Hadron Collider (LHC). Unlike GWs from strong astrophysical sources [91], these waves have a range between millihertz and decihertz [92]. The Laser Interferometer Space Antenna (LISA) [93] and Big Bang Observer (BBO) [94] are two space-based GW detectors which are expected to observe GWs resulting from cosmological phase transitions in future years. On the other hand, one of the Sakharov conditions [95] which explains the matter–antimatter asymmetry in universe

[a] e-mail: mojtaba_hosseini@semnan.ac.ir
[b] e-mail: syaser.ayazi@semnan.ac.ir (corresponding author)
[c] e-mail: mohamadnejad.a@lu.ac.ir

is the thermal imbalance that occurs in first-order phase transitions.

As mentioned, one of the fundamental challenges of particle physics is the hierarchy problem. A potential solution to this problem is to drop the Higgs mass term in the potential. SM without the Higgs mass term is scale-invariant. In this paper, we present a classically scale-invariant extension of the SM where all the particle masses are generated using the Coleman-Weinberg mechanism [96]. The model includes three new fields: a fermion, a complex singlet scalar and a vector field with $U_D(1)$ gauge symmetry. We examine two scenarios in this paper. In scenario A, we consider only the fermionic field as DM. In scenario B, both fermionic and vector fields are considered as DM. We probe the parameter space of the model according to constraints from relic density and direct detection. DM relic density is reported by the Planck Collaboration [97] and DM-Nucleon cross section is constrained by XENONnT experiment results [98]. We investigate the possibility of the electroweak phase transition with respect to the bounded parameter space, where we use the effects of the effective potential of the finite temperature. We probe the parameter space of the model, which is consistent with the said phenomenological constraints and also leads to a strong first-order electroweak phase transition. The GW signal resulting from this phase transition also has been studied in the LISA and BBO detectors.

Here is the organization of the paper. In the next section, we introduce the model. In Sect. 3, we study the phenomenology of the Scenario A including relic density, direct detection, invisible Higgs decay and the resulting GWs. Section 4 is dedicated to the phenomenology of the Scenario B and its GW signals. Finally, our conclusion comes in Sect. 5.

2 The model

In this section, we consider an extension of the SM to explain DM phenomenology. In this regard, the model contains three new fields in which a vector dark matter V_μ and a Dirac fermion field ψ can play the role of DM. A complex scalar, S, mediates between SM and the dark sector. In the model V_μ, ψ and S are charged under a new dark $U(1)_D$ gauge group. All of these fields are singlet under SM gauge groups. We suppose the mass of the fermion was produced by breaking of dark $U_D(1)$ gauge symmetry, and so was constrained by other parameters of the model. However, in the model, the dark sector is invariant under the transformations of the $U_D(1)$ gauge group:

$$\begin{aligned} &\psi_L \to e^{iQ_l\alpha(x)}\psi_L, \quad \psi_R \to e^{iQ_r\alpha(x)}\psi_R, \\ &S \to e^{iQ_s\alpha(x)}S, \quad V_\mu \to V_\mu - \frac{1}{g_v}\partial_\mu\alpha(x), \end{aligned} \tag{2.1}$$

Table 1 The charges of the dark sector particles under the new $U(1)_D$ symmetry

Field	S	ψ_L	ψ_R
$U(1)_D$ charge	1	$\frac{1}{2}$	$-\frac{1}{2}$

where the $U(1)_D$ charge of the new particles, $Q_{l,r,s}$, are given in Table 1.

The Lagrangian for the model is given by the following renormalizable interactions,

$$\begin{aligned} \mathcal{L} = \mathcal{L}_{\rm SM} + i\bar{\psi}_L\gamma^\mu D_\mu\psi_L + i\bar{\psi}_R\gamma^\mu D_\mu\psi_R - g_s\bar{\psi}_L\psi_R S \\ + h.c. - \frac{1}{4}V_{\mu\nu}V^{\mu\nu} + (D_\mu S)^*(D^\mu S) - V(H,S), \end{aligned} \tag{2.2}$$

where $\mathcal{L}_{\rm SM}$ is the SM Lagrangian without the Higgs potential term, The covariant derivative is

$$\begin{aligned} &D_\mu = (\partial_\mu + iQg_vV_\mu), \quad \text{and} \\ &V_{\mu\nu} = \partial_\mu V_\nu - \partial_\nu V_\mu. \end{aligned} \tag{2.3}$$

On the imposition of dark charge conjugation symmetry, we do not assume a kinetic mixing term between V_μ and the $U(1)_Y$ gauge boson of the SM.

The most general scale-invariant potential $V(H, S)$ that is renormalizable and invariant under gauge symmetry is

$$V(H,S) = \frac{1}{6}\lambda_H(H^\dagger H)^2 + \frac{1}{6}\lambda_S(S^*S)^2 + 2\lambda_{SH}(S^*S)(H^\dagger H). \tag{2.4}$$

Note that the quartic portal interaction, $\lambda_{SH}(S^*S)(H^\dagger H)$, is the only connection between the dark sector and the SM.

SM Higgs field H as well as dark scalar S can receive VEVs, respectively breaking the electroweak and $U_D(1)$ symmetries. In unitary gauge, the imaginary component of S can be absorbed as the longitudinal part of V_μ. In this gauge, we can write

$$H = \frac{1}{\sqrt{2}}\begin{pmatrix} 0 \\ h_1 \end{pmatrix} \quad \text{and} \quad S = \frac{1}{\sqrt{2}}h_2, \tag{2.5}$$

where h_1 and h_2 are real scalar fields which can receive VEVs. Now, the tree-level potential becomes

$$V^{\rm tree} = \frac{1}{4!}\lambda_H h_1^4 + \frac{1}{4!}\lambda_S h_2^4 + \frac{1}{2}\lambda_{SH}h_1^2h_2^2. \tag{2.6}$$

There is a Z_2 symmetry for ψ, making it a stable particle. In addition, if the mass of V_μ is less than two times of the mass of ψ, then both V_μ and ψ are viable DM candidates.

For the Hessian matrix, we define:

$$H_{ij}(h_1, h_2) \equiv \frac{\partial^2 V^{\text{tree}}}{\partial h_i \partial h_j}. \tag{2.7}$$

Necessary and sufficient conditions for local minimum of V^{tree} in which vacuum expectation values $\langle h_1 \rangle = v_1$ and $\langle h_2 \rangle = v_2$, have been written as:

$$\left.\frac{\partial V^{\text{tree}}}{\partial h_i}\right|_{v_1, v_2} = 0 \tag{2.8}$$

$$\left.\frac{\partial^2 V^{\text{tree}}}{\partial h_i^2}\right|_{v_1, v_2} > 0 \tag{2.9}$$

$$\det(H(v_1, v_2)) > 0, \tag{2.10}$$

where $\det(H(v_1, v_2))$ is the determinant of the Hessian matrix. Condition (2.8) for non-vanishing VEVs leads to the following constraints:

$$\lambda_H \lambda_S = (3!\lambda_{SH})^2 \qquad \frac{v_1^2}{v_2^2} = -\frac{3!\lambda_{SH}}{\lambda_H}. \tag{2.11}$$

Conditions (2.8) and (2.9) require $\lambda_H > 0$, $\lambda_S > 0$, and $\lambda_{SH} < 0$. However, condition (2.10) will not be satisfied, because $\det(H(v_1, v_2)) = 0$. When the determinant of the Hessian matrix is zero, the second derivative test is inconclusive, and the point (v_1, v_2) could be any of a minimum, maximum or saddle point. However, in the model, constraint (2.11) is defined as a flat direction, in which $V^{\text{tree}} = 0$. Thus, it is the stationary line or a local minimum.

The important point is that for other directions, $V_{\text{eff}}^{1-\text{loop}(T=0)} > 0$, and the tree level potential only vanishes along the flat direction. Thus, the full potential of the theory will be dominated by higher-loop contributions along the flat direction, and specifically by the one-loop effective potential. Considering one-loop effective potential, $V_{\text{eff}}^{1-\text{loop}}$, can lead to a small curvature in the flat direction, which picks out a specific value along the ray as the minimum with $V_{\text{eff}}^{1-\text{loop}} < 0$ and vacuum expectation value $v^2 = v_1^2 + v_2^2$ characterized by a renormalization group (RG) scale Λ. Since at the minimum of the one-loop effective potential $V^{\text{tree}} \geqslant 0$ and $V_{\text{eff}}^{1-\text{loop}} < 0$, the minimum of $V_{\text{eff}}^{1-\text{loop}}$ along the flat direction (where $V^{\text{tree}} = 0$) is a global minimum of the full potential, and so spontaneous symmetry breaking takes place. As a result, we suppose $h_1 \to v_1 + h_1$ and $h_2 \to v_2 + h_2$, and the electroweak symmetry breaks with value $v_1 = 246$ GeV. In tree level potential, since h_1 and h_2 mix with each other, they can be rewritten by the mass eigenstates H_1 and H_2 as

$$\begin{pmatrix} H_1 \\ H_2 \end{pmatrix} = \begin{pmatrix} \cos\alpha & -\sin\alpha \\ \sin\alpha & \cos\alpha \end{pmatrix} \begin{pmatrix} h_1 \\ h_2 \end{pmatrix}, \tag{2.12}$$

where H_2 is along the flat direction; thus $M_{H_2} = 0$, and H_1 is perpendicular to the flat direction which we identify as the SM-like Higgs observed at the LHC with $M_{H_1} = 125$ GeV. After the symmetry breaking, we have the following constraints:

$$\begin{aligned} v_2 &= \frac{M_V}{g_v}, \quad \sin\alpha = \frac{v_1}{\sqrt{v_1^2 + v_2^2}} \\ M_\psi &= \frac{g_s M_V}{\sqrt{2} g_v} \quad \lambda_H = \frac{3M_{H_1}^2}{v_1^2}\cos^2\alpha \\ \lambda_S &= \frac{3M_{H_1}^2}{v_2^2}\sin^2\alpha \quad \lambda_{SH} = -\frac{M_{H_1}^2}{2v_1 v_2}\sin\alpha\,\cos\alpha, \end{aligned} \tag{2.13}$$

where M_ψ and M_V are the masses of vector and fermion fields after symmetry breaking. Conditions (2.13) constrain free parameters of the model up to three independent parameters. We choose M_V, M_ψ and g_v as the independent parameters of the model.

Since in tree level, $M_{H_2} = 0$, and the elastic scattering cross section of DM off nuclei becomes severely large, the model actually is excluded by direct detection experiments. However, the radiative corrections give a mass to the massless eigenstate H_2. One-loop corrections to the potential, via the Gildener–Weinberg formalism [99], shift the scalon mass to the values that can be even higher than SM Higgs mass. Along the flat direction, the one-loop effective potential has the general form [99]

$$V_{\text{eff}}^{1-\text{loop}(T=0)} = aH_2^4 + bH_2^4 \ln\frac{H_2^2}{\Lambda^2}, \tag{2.14}$$

where a and b are dimensionless constants that given by

$$\begin{aligned} a &= \frac{1}{64\pi^2 v^4}\sum_{k=1}^{n} g_k M_k^4 \ln\frac{M_k^2}{v^2}, \\ b &= \frac{1}{64\pi^2 v^4}\sum_{k=1}^{n} g_k M_k^4. \end{aligned} \tag{2.15}$$

In (2.15), M_k and g_k are the tree-level mass and the internal degrees of freedom of the particle k, respectively (In our convention g_k takes positive values for bosons and negative values for fermions).

Minimizing (2.14) shows that the potential has a non-trivial stationary point at a value of the RG scale Λ, given by

$$\Lambda = v \exp\left(\frac{a}{2b} + \frac{1}{4}\right). \tag{2.16}$$

Equation (2.16) can now be used to find the form of the one-loop effective potential along the flat direction in terms of

the one-loop VEV v:

$$V_{\text{eff}}^{1-\text{loop}(T=0)} = bH_2^4\left(\ln\frac{H_2^2}{v^2} - \frac{1}{2}\right). \tag{2.17}$$

It is noteworthy that the scalon does not remain massless beyond the tree approximation. Regarding $V_{\text{eff}}^{1-\text{loop}(T=0)}$, M_{H_2} will be

$$M_{H_2}^2 = \left.\frac{d^2V_{\text{eff}}^{1-\text{loop}(T=0)}}{dH_2^2}\right|_v = 8bv^2. \tag{2.18}$$

Considering (2.15), the scalon mass can be expressed in terms of other particle masses

$$M_{H_2}^2 = \frac{1}{8\pi^2v^2}\left(M_{H_1}^4 + 6M_W^4 + 3M_Z^4 + 3M_V^4 - 12M_t^4 - 4M_\psi^4\right), \tag{2.19}$$

where $M_{W,Z,t}$ are the masses of W, Z gauge bosons, and top quark, respectively. As mentioned before, $M_{H_1} = 125$ GeV and $v^2 = v_1^2 + v_2^2$. Notice that in order for $V_{\text{eff}}^{1-\text{loop}(T=0)}$ to be a minimum, it must be less than the value of the potential at the origin, hence it must be negative. From (2.19), we have a constraint on the parameter space of our model where $M_{H_2} > 0$.

Note that according to (2.19) and (2.13), M_{H_2} is completely determined by the independent parameters of the model, i.e., M_V, M_ψ and the coupling g_v. These constraints are due to the scale invariance conditions which were imposed on the model. Depending on the new particle masses of our model, we examine two different scenarios. In scenario A, the ψ field is considered as DM. In scenario B, $M_V < 2M_\psi$ and both V_μ and ψ fields are considered as DM. In the following, we examine the phenomenology of each scenario separately.

3 Scenario A

3.1 DM phenomenology

3.1.1 Relic density

In this case, since we do not assume $M_V < 2M_\psi$, the only candidate for DM is ψ. In the WIMP scenario, at first the early universe is hot and very dense and all particles are in thermal equilibrium. Then the universe cools until its temperature falls below the mass of DM particles, and the amount of DM becomes Boltzmann suppressed, dropping exponentially as $e^{-m_X/T}$. As the universe expands, the DM particles are diluted and can no longer find each other until they are annihilated and are out of thermal equilibrium with the SM particles. Then the DM particles freeze out and their number asymptotically reaches a constant value as their thermal relic density. The evolution of the number density of DM particle (n_ψ) with time is governed by the Boltzmann equation:

$$\dot{n_\psi} + 3Hn_\psi = -\langle\sigma_{\text{ann}}v_{\text{rel}}\rangle[n_\psi^2 - (n_\psi^{\text{eq}})^2], \tag{3.1}$$

where H is the Hubble parameter and $n_\psi^{\text{eq}} \sim (m_\psi T)^{3/2} e^{-m_\psi/T}$ is the particle density before particles get out of equilibrium. The relevant Feynman diagrams for DM production are shown in the Fig. 1. We calculate the relic density numerically for the ψ particle by implementing the model into micrOMEGAs [100]. Figure 2 shows the parameter space of the model in agreement with the observed density relic [97]. As can be seen, there is agreement for $400 < M_V < 5000$ GeV, $20 < M_\psi < 2500$ GeV and $0.1 < g_v < 6$.

3.1.2 Direct detection

WIMPs may be detected by the scattering off normal matter through processes $XSM \to XSM$. Given a typical WIMP mass of $m_X \sim 100$ GeV and WIMP velocity $v \sim 10^{-3}$, the deposited recoil energy is limited to ~ 100 keV, so detection requires highly-sensitive, low-background and deep-site detectors. Such detectors are insensitive to very strongly-interacting DM, which would be stopped in the atmosphere or earth and would be undetectable underground. The spin-independent direct detection(DD) cross sections of ψ were obtained using the micrOMEGAs package [100].

In Fig. 3, the parameter space of the model is drawn in agreement with the limits of relic density, XENONnT and neutrino floor. For $20 < M_\psi < 1000$ GeV, there will be points of the parameter space that fall below the XENONnT limit. As can be seen from Fig. 3, for $M_\psi < M_{H_1}/2$ there will be points that allow the investigation of the invisibility Higgs decay, which will be investigated in the next section.

3.1.3 Invisible Higgs decay

As mentioned, for a parameter space consistent with ψ relic density and DD, SM Higgs(H_1) can only kinematically decay into a pair of ψ. Therefore, H_1 can contribute to the invisible decay mode with a branching ratio:

$$Br(H_1 \to \text{Invisible}) = \frac{\Gamma(\text{H}_1 \to \psi\psi)}{\Gamma(\text{h})_{\text{SM}} + \Gamma(\text{H}_1 \to \psi\psi)}, \tag{3.2}$$

where $\Gamma(h)_{SM} = 4.15$ [MeV] is total width of Higgs boson [101]. The partial width for process $H_1 \to \psi\psi$ is given by:

$$\Gamma(H_1 \to \psi\psi) = \frac{M_{H_1}g_s^2\sin^2\theta}{8\pi}\left(1 - \frac{4M_\psi^2}{M_{H_1}^2}\right)^{3/2}. \tag{3.3}$$

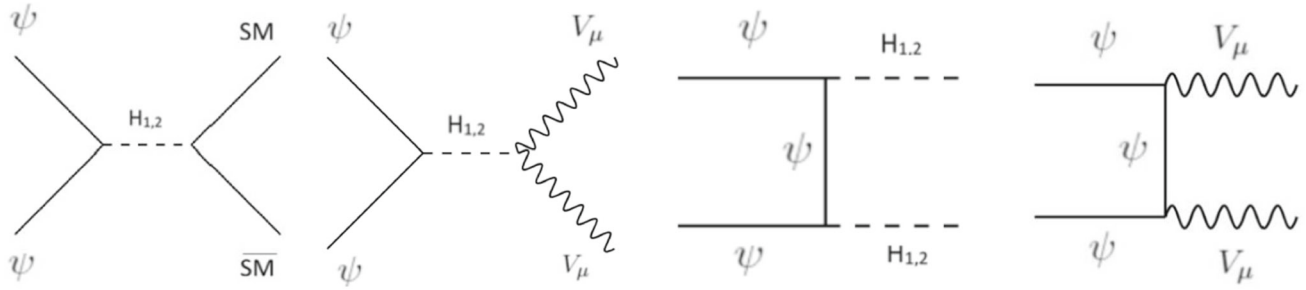

Fig. 1 The relevant Feynman diagrams for DM relic density production cross section

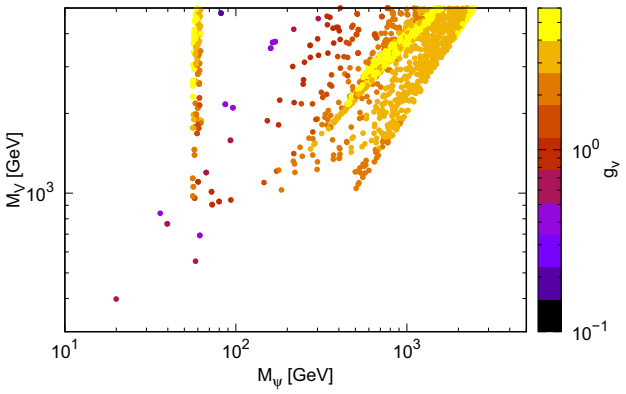

Fig. 2 The allowed range of parameter space consistent with DM relic density

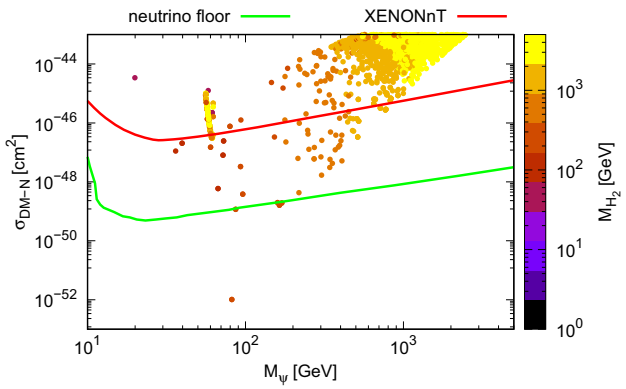

Fig. 3 The allowed range of parameter space consistent with DM relic density and DD

The SM prediction for the branching ratio of the Higgs boson decaying to invisible particles coming from process $h \to ZZ^* \to 4\nu$ [102–105] is 1.2×10^{-3}. CMS Collaboration has reported the observed (expected) upper limit on the invisible branching fraction of the Higgs boson to be 0.18(0.10) at the 95% confidence level, by assuming the SM production cross section [106]. A similar analysis was performed by ATLAS collaboration in which an observed upper limit of 0.145 is placed on the branching fraction of its decay into invisible particles at a 95% confidence level [107].

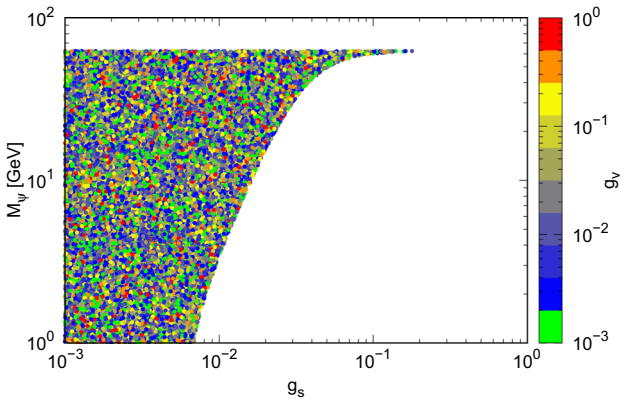

Fig. 4 The cross points depict the allowed region that is consistent with invisible Higgs decay at [107]

Figure 4, shows the allowed range of parameters by considering the ATLAS [107] upper limit for invisible Higgs mode.

3.2 Electroweak phase transition and gravitational waves

3.2.1 Finite temperature potential

In addition to the 1-loop zero-temperature potential (2.17), we can also consider the 1-loop corrections at finite temperature in the effective potential, which is [108]

$$V_{\text{eff}}^{1-\text{loop}(T\neq 0)}(H_2, T) = \frac{T^4}{2\pi^2} \sum_{k=1}^{n} g_k J_{B,F}\left(\frac{M_k}{\nu}\frac{H_2}{T}\right), \quad (3.4)$$

with thermal functions

$$J_{B,F}(x) = \int_0^\infty dy y^2 \ln\left(1 \mp e^{-\sqrt{y^2+x^2}}\right). \quad (3.5)$$

The above functions can be expanded in terms of modified Bessel functions of the second kind, $K_2(x)$ [71],

$$J_B(x) \simeq -\sum_{k=1}^{3} \frac{1}{k^2} x^2 K_2(kx),$$
$$J_F(x) \simeq -\sum_{k=1}^{2} \frac{(-1)^k}{k^2} x^2 K_2(kx). \tag{3.6}$$

The contribution of resummed daisy graphs is also as follows [109]

$$V_{\text{daisy}}(H_2, T) = \sum_{k=1}^{n} \frac{g_k T^4}{12\pi} \left(\left(\frac{M_k}{\nu} \frac{H_2}{T} \right)^3 - \left(\left(\frac{M_k}{\nu} \frac{H_2}{T} \right)^2 + \frac{\Pi_k(T)}{T^2} \right)^{\frac{3}{2}} \right), \tag{3.7}$$

where the sum runs only over scalar bosons and longitudinal degrees of freedom of the gauge bosons. Thermal masses, $\Pi_k(T)$, are given by

$$\Pi_W = \frac{11}{6} g_{SM}^2 T^2, \quad \Pi_V = \frac{2}{3} g_v^2 T^2,$$
$$\Pi_{Z/\gamma} = \frac{11}{6} \begin{pmatrix} g_{SM}^2 & 0 \\ 0 & g_{SM}'^2 \end{pmatrix} T^2,$$
$$\Pi_{H_1/H_2} = \begin{pmatrix} \frac{\lambda_H}{24} + \frac{\lambda_{SH}}{12} + \frac{3g_{SM}^2}{16} + \frac{g_{SM}'^2}{16} + \frac{\lambda_t^2}{4} & 0 \\ 0 & \frac{\lambda_S}{24} + \frac{\lambda_{SH}}{12} + \frac{g_v^2}{4} \end{pmatrix} T^2. \tag{3.8}$$

Finally, the one-loop effective potential, including both one-loop zero temperature (2.17) and finite temperature (3.4) and 3.7 corrections, is given by

$$V_{\text{eff}}(H_2, T) = V^{1-\text{loop}(T=0)}(H_2) + V^{1-\text{loop}(T\neq 0)}(H_2, T) + V_{\text{daisy}}(H_2, T). \tag{3.9}$$

In order to get $V_{\text{eff}}(0, T) = 0$ at all temperatures, we make the following substitution:

$$V_{\text{eff}}(H_2, T) \longrightarrow V_{\text{eff}}(H_2, T) - V_{\text{eff}}(0, T). \tag{3.10}$$

Now we are ready to study the phase transition and the resulting gravitational waves.

3.2.2 Gravitational waves

The characteristic of first-order phase transitions is the existence of a barrier between the symmetric and broken phases. The electroweak phase transition takes place after the temperature of the universe drops below the critical temperature (T_C). At this temperature, effective potential (3.9) has two degenerate minimums, one in $H_2 = 0$ and the other in $H_2 = \nu_C \neq 0$:

$$V_{\text{eff}}(0, T_C) = V_{\text{eff}}(\nu_C, T_C),$$
$$\left. \frac{\mathrm{d}V_{\text{eff}}(H_2, T_C)}{\mathrm{d}H_2} \right|_{H_2=\nu_C} = 0. \tag{3.11}$$

By solving these two equations, one can obtain ν_C and T_C. If this phase transition is strongly first-order, it can satisfy the condition of departure from thermal equilibrium, which is one of Sakharov conditions for creating baryonic asymmetry in the universe. There is a criteria for strongly electroweak phase transition [95,110], which is as follows

$$\frac{\nu_C}{T_C} > 1. \tag{3.12}$$

The transition from the false to the true vacuum proceeds via thermal tunneling at finite temperature. This concept can be grasped in the context of formation of bubbles of the broken phase in the sea of the symmetric phase. Once this has happened, the bubble spreads throughout the universe, converting false vacuums into true ones. Bubble formation starts at the nucleation temperature T_N, where one can estimate T_N by the condition $S_3(T_N)/T_N \sim 140$ [111]. The function $S_3(T)$ is the three-dimensional Euclidean action for a spherical symmetric bubble given by

$$S_3(T) = 4\pi \int_0^\infty \mathrm{d}r r^2 \left(\frac{1}{2} \left(\frac{\mathrm{d}H_2}{\mathrm{d}r} \right)^2 + V_{eff}(H_2, T) \right), \tag{3.13}$$

where H_2 satisfies the differential equation which minimizes S_3:

$$\frac{\mathrm{d}^2 H_2}{\mathrm{d}r^2} + \frac{2}{r} \frac{\mathrm{d}H_2}{\mathrm{d}r} = \frac{\mathrm{d}V_{\text{eff}}(H_2, T)}{\mathrm{d}H_2}, \tag{3.14}$$

with the boundary conditions:

$$\left. \frac{\mathrm{d}H_2}{\mathrm{d}r} \right|_{r=0} = 0, \quad \text{and} \quad H_2(r \longrightarrow \infty) = 0. \tag{3.15}$$

In order to solve Eq. 3.14 and find the Euclidean action (3.13), we used the AnyBubble package [112]. In the following, we will show that the nucleation temperature(T_N) will be much lower than the critical temperature (T_C), indicating a very strong phase transition.

GWs resulting from the strong first-order electroweak phase transitions are have three causes, which are as follows:

- collisions of bubble walls and shocks in the plasma,
- sound waves to the stochastic background after collision of bubbles but before expansion has dissipated the kinetic energy in the plasma,

- turbulence forming after bubble collisions.
  These three processes may coexist, and each one contributes to the stochastic GW background:

$$\Omega_{\rm GW}h^2 \simeq \Omega_{\rm coll}h^2 + \Omega_{\rm sw}h^2 + \Omega_{\rm turb}h^2. \tag{3.16}$$

There are four thermal parameters that control the above contributions:

- T_N: the nucleation temperature,
- α: the ratio of the free energy density difference between the true and false vacuum and the total energy density,

$$\alpha = \frac{\Delta\Big(V_{\rm eff} - T\frac{\partial V_{\rm eff}}{\partial T}\Big)\Big|_{T_N}}{\rho_*}, \tag{3.17}$$

where ρ_* is

$$\rho_* = \frac{\pi^2 g_*}{30}T_N^4, \tag{3.18}$$

- β: the inverse time duration of the phase transition,

$$\frac{\beta}{H_*} = T_N\frac{\rm d}{{\rm d}T}\Big(\frac{S_3(T)}{T}\Big)\Big|_{T_N}, \tag{3.19}$$

- υ_ω: the velocity of the bubble wall which is anticipated to be close to 1 for the strong transitions [113].

Isolated spherical bubbles cannot be used as a source of GWs, and these waves arise during the collision of the bubbles. The collision contribution to the spectrum is given by [114]

$$\Omega_{\rm coll}(f)h^2 = 1.67\times10^{-5}\Big(\frac{\beta}{H_*}\Big)^{-2} \times\Big(\frac{\kappa\alpha}{1+\alpha}\Big)^2\Big(\frac{g_*}{100}\Big)^{-\frac{1}{3}}\Big(\frac{0.11\upsilon_\omega^3}{0.42+\upsilon_\omega^2}\Big)S_{\rm coll}, \tag{3.20}$$

where $S_{\rm coll}$ parameterizes the spectral shape and is given by

$$S_{\rm coll} = \frac{3.8(f/f_{\rm coll})^{2.8}}{2.8(f/f_{\rm coll})^{3.8}+1}, \tag{3.21}$$

where

$$f_{\rm coll} = 1.65\times10^{-5}\Big(\frac{0.62}{\upsilon_\omega^2 - 0.1\upsilon_\omega + 1.8}\Big)\Big(\frac{\beta}{H_*}\Big) \times\Big(\frac{T_N}{100}\Big)\Big(\frac{g_*}{100}\Big)^{1/6}Hz. \tag{3.22}$$

The collision of bubbles produces a massive movement in the fluid in the form of sound waves that generate GWs. This is the dominant contribution to the GW signal, and is given by [115]

$$\Omega_{\rm sw}(f)h^2 = 2.65\times10^{-6}\Big(\frac{\beta}{H_*}\Big)^{-1}\Big(\frac{\kappa_\upsilon\alpha}{1+\alpha}\Big)^2 \times\Big(\frac{g_*}{100}\Big)^{-\frac{1}{3}}\upsilon_\omega S_{\rm sw}. \tag{3.23}$$

The spectral shape of $S_{\rm sw}$ is

$$S_{\rm sw} = (f/f_{\rm sw})^3\Big(\frac{7}{3(f/f_{\rm sw})^2+4}\Big)^{3.5}, \tag{3.24}$$

where

$$f_{\rm sw} = 1.9\times10^{-5}\frac{1}{\upsilon_\omega}\Big(\frac{\beta}{H_*}\Big)\Big(\frac{T_N}{100}\Big)\Big(\frac{g_*}{100}\Big)^{1/6}Hz. \tag{3.25}$$

Plasma turbulence can also be caused by bubble collisions, which is a contributing factor to the GW spectrum and is given by [116]

$$\Omega_{\rm turb}(f)h^2 = 3.35\times10^{-4}\Big(\frac{\beta}{H_*}\Big)^{-1}\Big(\frac{\kappa_{turb}\alpha}{1+\alpha}\Big)^{3/2} \times\Big(\frac{g_*}{100}\Big)^{-\frac{1}{3}}\upsilon_\omega S_{turb}, \tag{3.26}$$

where

$$S_{\rm turb} = \frac{(f/f_{turb})^3}{(1+8\pi f/h_*)(1+f/f_{\rm turb})^{11/3}}, \tag{3.27}$$

and

$$f_{\rm turb} = 2.27\times10^{-5}\frac{1}{\upsilon_\omega}\Big(\frac{\beta}{H_*}\Big)\Big(\frac{T_N}{100}\Big)\Big(\frac{g_*}{100}\Big)^{1/6}Hz. \tag{3.28}$$

In Eq. 3.27, h_* is the value of the inverse Hubble time at GW production, redshifted to today,

$$h_* = 1.65\times10^{-5}\Big(\frac{T_N}{100}\Big)\Big(\frac{g_*}{100}\Big)^{1/6}. \tag{3.29}$$

In computing the GW spectrum we have used [117,118]

$$\kappa = \frac{1}{1+0.715\alpha}\Big(0.715\alpha + \frac{4}{27}\sqrt{\frac{3\alpha}{2}}\Big), \quad \kappa_\upsilon = \frac{\alpha}{0.73+0.083\sqrt{\alpha}+\alpha}, \quad \kappa_{\rm turb} = 0.05\kappa_\upsilon, \tag{3.30}$$

where the parameters κ, κ_υ, and $\kappa_{\rm turb}$ denote the fraction of latent heat that is transformed into gradient energy of the Higgs-like field, bulk motion of the fluid, and MHD turbulence, respectively.

To investigate the GWs resulting from the first-order electroweak phase transition, we choose three benchmark points. These points are presented in Table 2. Figure 5 shows the

Table 2 Three benchmark points with DM and phase transition parameters

#	M_V (GeV)	M_ψ (GeV)	g_v	g_s	M_{H_2} (GeV)	$\Omega_\psi h^2$	σ_ψ (cm^2)
1	839.9	36.1	0.485	0.029	78.39	1.11×10^{-1}	1.11×10^{-47}
2	4998	407.8	0.87	0.1	849.1	1.18×10^{-1}	5.16×10^{-48}
3	3526	159.7	0.468	0.029	321.6	1.2×10^{-1}	1.98×10^{-49}
#	T_C (GeV)	T_N (GeV)	α	β/H_*	$(\Omega_{\rm GW}h^2)_{\rm max}$		
1	237	71	1.48	306.694	1.32×10^{-9}	–	–
2	1665	1490.7	0.02	2758.95	2.68×10^{-16}	–	–
3	1114	640.8	0.09	244.78	8.77×10^{-13}	–	–

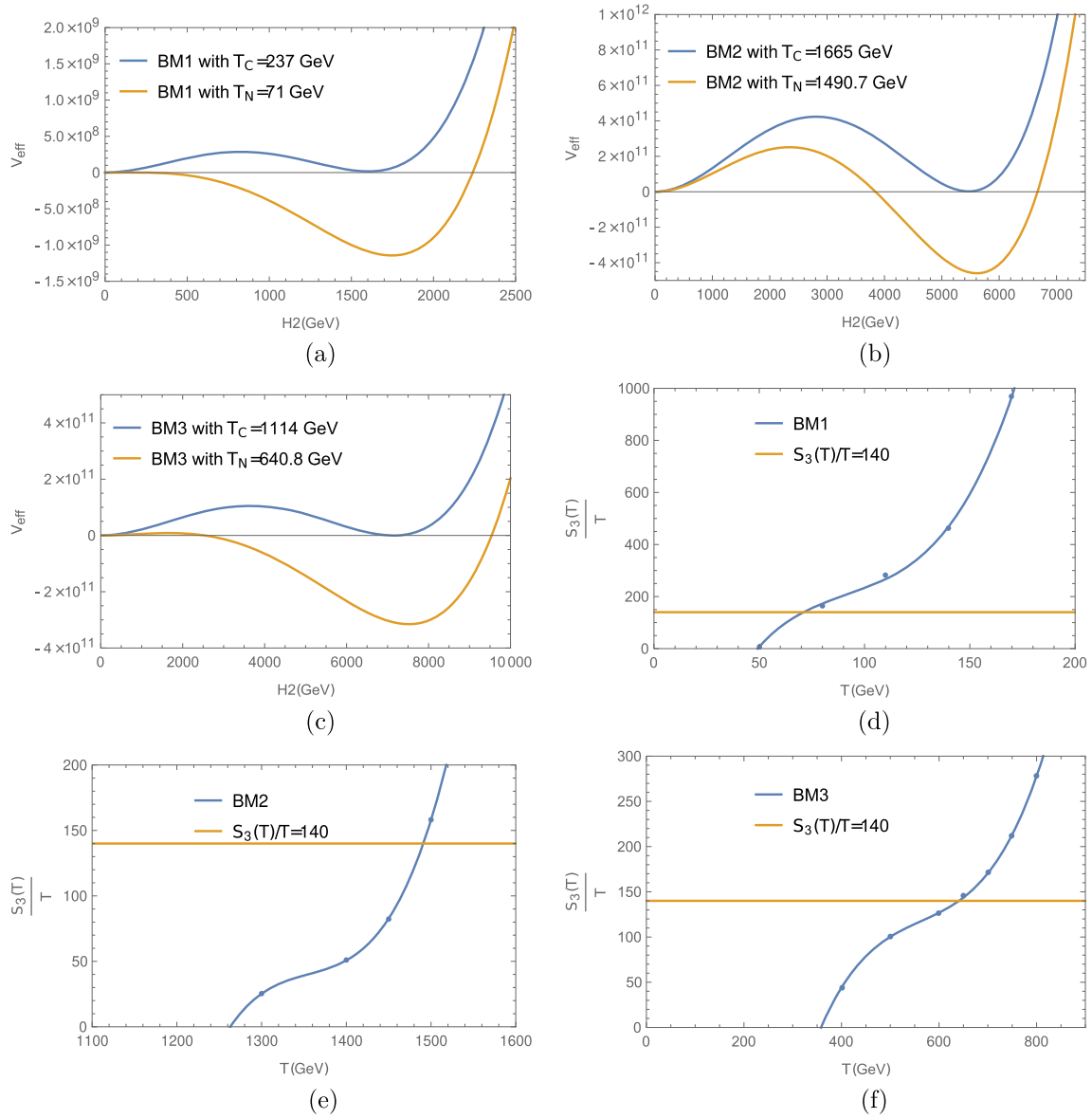

Fig. 5 In **a**, **b** and **c** Potential behavior are given for critical temperature and nucleation temperature. In **d**, **e** and **f** S_3/T changes in terms of temperature are also given for all three benchmarks

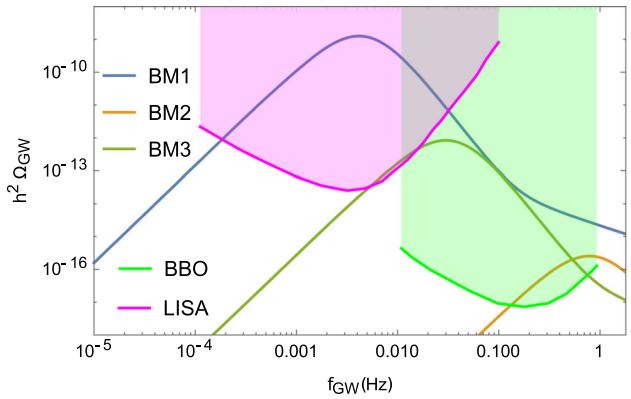

Fig. 6 GW spectrum for benchmark points of the Table 2

potential behavior for both critical and nucleation temperatures. Also, S_3/T changes in terms of temperature are shown. In Table 2 all relevant quantities, including independent parameters of the model, DM properties, and phase transition parameters, are given. The benchmarks 1 and 2 are consistent with direct detection constraints while benchmark 3 is outside the range of XENONnT and is placed under the neutrino floor. The GW spectrum for these benchmark points is depicted in Fig. 6. The GW spectrum for these benchmarks 1,(2,3) falls within the observational window of LISA(BBO). Therefore, for benchmark 3, GW can be a special way to probe it.

4 Scenario B

4.1 DM phenomenology

4.1.1 Relic density

In this scenario, $M_V < 2M_\psi$ and both V_μ and ψ fields are considered as DM. The evolution of the number density of DM particles with time are governed by the Boltzmann equation. The coupled Boltzmann equations for fermion ψ and vector DM are given by:

$$\frac{dn_V}{dt} + 3Hn_V = -\sum_j \langle\sigma_{VV\to jj}\upsilon\rangle(n_V^2 - n_{V,\text{eq}}^2) - \langle\sigma_{VV\to\psi\psi}\upsilon\rangle\left(n_V^2 - n_{V,\text{eq}}^2\frac{n_\psi^2}{n_{\psi,\text{eq}}^2}\right), \tag{4.1}$$

$$\frac{dn_\psi}{dt} + 3Hn_\psi = -\sum_j \langle\sigma_{\psi\psi\to jj}\upsilon\rangle(n_\psi^2 - n_{\psi,\text{eq}}^2) - \langle\sigma_{\psi\psi\to VV}\upsilon\rangle\left(n_\psi^2 - n_{\psi,\text{eq}}^2\frac{n_V^2}{n_{V,\text{eq}}^2}\right), \tag{4.2}$$

where j runs over SM massive particles, H_1 and H_2. In $\langle\sigma_{ab\to cd}\upsilon\rangle$ all annihilations are taken into account except $\langle\sigma_{\psi V\to\psi V}\upsilon\rangle$ which does not affect the number density. In the above relations, for simplicity in the writing, only the annihilation and conversion contributions are shown in the equations. But, in practice, all contributions, even semi-annihilations are included in the micrOMEGAs package to solve these equations [119]. The relevant Feynman diagrams for DM production are shown in Fig. 7. By choosing $x = M/T$ and $Y = n/s$,, where T and s are the photon temperature and the entropy density, respectively, one can rewrite the Boltzmann equations in terms of $Y = n/s$:

$$\frac{dY_V}{dx} = -\sqrt{\frac{45}{\pi}}M_{pl}g_*^{1/2}\frac{M}{x^2}\left[\sum_j\langle\sigma_{VV\to jj}\upsilon\rangle(Y_V^2 - Y_{V,\text{eq}}^2) + \langle\sigma_{VV\to\psi\psi}\upsilon\rangle\left(Y_V^2 - Y_{V,\text{eq}}^2\frac{Y_\psi^2}{Y_{\psi,\text{eq}}^2}\right)\right], \tag{4.3}$$

$$\frac{dY_\psi}{dx} = -\sqrt{\frac{45}{\pi}}M_{pl}g_*^{1/2}\frac{M}{x^2}\left[\sum_j\langle\sigma_{\psi\psi\to jj}\upsilon\rangle(Y_\psi^2 - Y_{\psi,\text{eq}}^2) + \langle\sigma_{\psi\psi\to VV}\upsilon\rangle\left(Y_\psi^2 - Y_{\psi,\text{eq}}^2\frac{Y_V^2}{Y_{V,\text{eq}}^2}\right)\right], \tag{4.4}$$

where $g_*^{1/2}$ is the degrees of freedom parameter and M_{pl} is the Planck mass. It is clear from the above equations that there are new terms in the Boltzmann equations that describe the conversion of two DM particles into each other. Because these two cross sections are also described by the same matrix element, we expect $\langle\sigma_{VV\to\psi\psi}\upsilon\rangle$ and $\langle\sigma_{\psi\psi\to VV}\upsilon\rangle$ are not independent and their relation is:

$$Y_{V,eq}^2\langle\sigma_{VV\to\psi\psi}\upsilon\rangle = Y_{\psi,eq}^2\langle\sigma_{\psi\psi\to VV}\upsilon\rangle. \tag{4.5}$$

The interactions between the two DM components take place by exchanging two scalar mass eigenstates H_1 and H_2, where the coupling of V to H_1 is suppressed by $\sin\alpha$. For this reason, it usually is the H_2-mediated diagram that gives the dominant contribution. We also know that the conversion of the heavier particle into the lighter one is relevant. The relic density for any DM candidate associated with Y at the present temperature is given by the following relation:

$$\Omega_{\psi,V}h^2 = 2.755\times10^8\frac{M_{\psi,V}}{GeV}Y_{\psi,V}(T_0), \tag{4.6}$$

where h is the Hubble expansion rate at present time in units of 100 (km/s)/Mpc. We used the micrOMEGAs package [119] to numerically solve coupled Boltzmann differential equations. According to the data from the Planck Collabora-

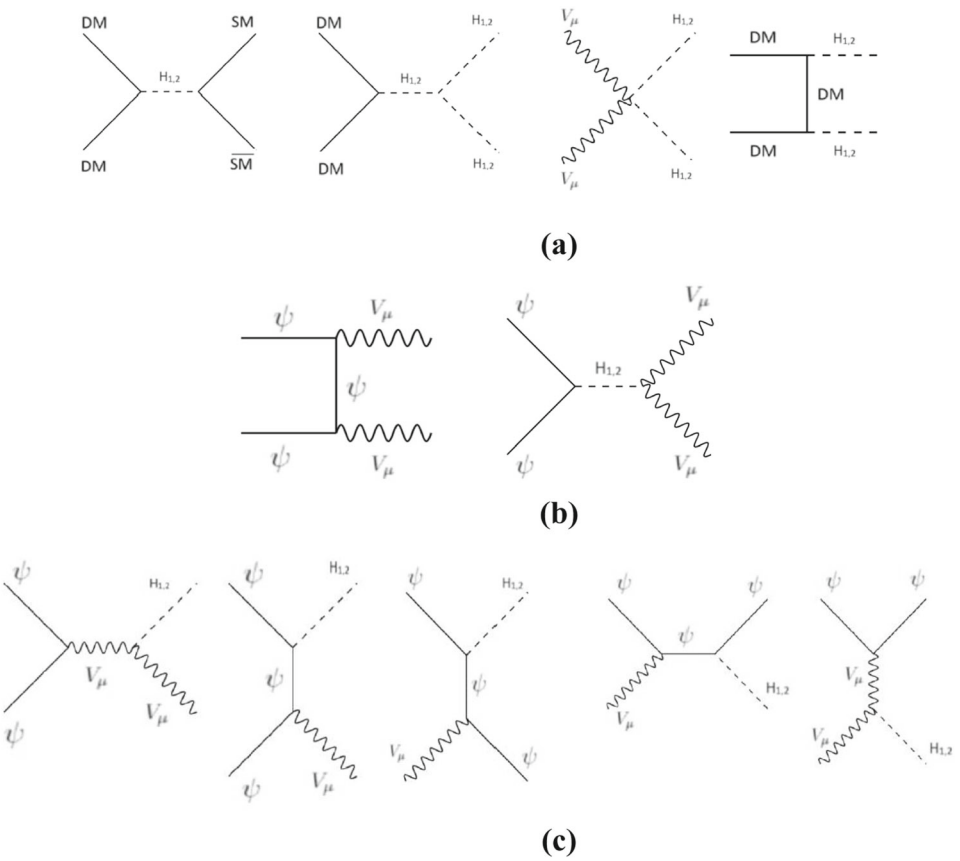

Fig. 7 The relevant Feynman diagrams for DM relic density cross section including: a (annihilation), b (conversion) and c (semi-annihilation)

tion [97], the DM constraint in this model reads

$$\Omega_{\rm DM}h^2 = \Omega_V h^2 + \Omega_\psi h^2 = 0.120 \pm 0.001. \tag{4.7}$$

We also define the fraction of the DM density of each component by

$$\xi_V = \frac{\Omega_V}{\Omega_{\rm DM}}, \quad \xi_\psi = \frac{\Omega_\psi}{\Omega_{\rm DM}}, \quad \xi_V + \xi_\psi = 1. \tag{4.8}$$

In Fig. 8, the parameter space consistent with DM relic density is obtained. As can be seen, there is an agreement with the relic density observed for $300 < M_V < 5000$ GeV, $200 < M_\psi < 5000$ GeV and $0.1 < g_v < 6$. Of course, it is necessary to mention that the contribution of semi-annihilations in the model is important. For example, for benchmark 2 in Table 3, using the micrOMEGAs package, we found that the share of the cross section of the process of V $\psi \to \psi\ H_2$ includes 24 % of the cross section of all processes.

4.1.2 Direct detection

We investigate constraints on parameters space of the model which are imposed by searching for scattering of DM-nuclei. The spin-independent direct detection (DD) cross sections of

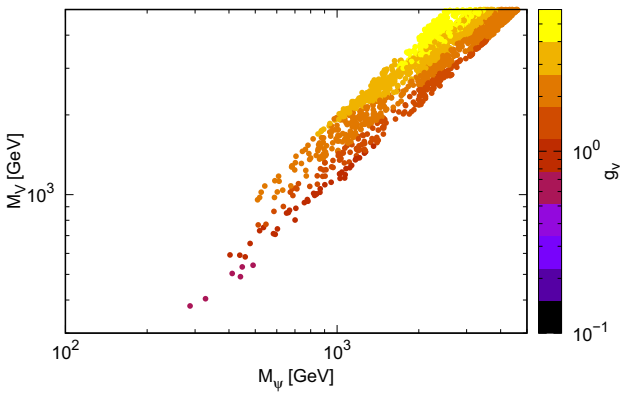

Fig. 8 The allowed range of parameter space consistent with DM relic density

V and ψ are determined by H_1 and H_2 exchanged diagrams [30,70]:

$$\sigma^V_{\rm DM-N} = \xi_V \frac{4\lambda^2_{SH} M_V^2 M_N^2 \mu^2_{VN} (M^2_{H1} - M^2_{H2})^2}{\pi M^8_{H1} M^4_{H2}} f_N^2, \tag{4.9}$$

$$\sigma^\psi_{\rm DM-N} = \xi_\psi \frac{g_s^3 v_1}{\pi M_\psi (1 + (v_1 g_s / M_\psi)^2)} \mu^2_\psi \times \left(\frac{1}{M^2_{H1}} - \frac{1}{M^2_{H2}}\right)^2 f_N^2, \tag{4.10}$$

Table 3 Three benchmark points with DM and phase transition parameters

#	$M_V(GeV)$	$M_\psi(GeV)$	g_v	g_s	$M_{H_2}(GeV)$
1	2249	2069	1.32	1.72	121.7
2	3400	3150	1.65	2.16	140
3	3750	3481	1.71	2.25	125.1
#	$\Omega_V h^2$	$\Omega_\psi h^2$	$\Omega_{DM} h^2$	$\xi_V \sigma_V$ (cm^2)	$\xi_\psi \sigma_\psi$ (cm^2)
1	1.17×10^{-2}	1.09×10^{-1}	1.2×10^{-1}	6.02×10^{-48}	4.75×10^{-47}
2	1.1×10^{-2}	9.99×10^{-2}	1.1×10^{-1}	9.03×10^{-47}	7.04×10^{-46}
3	1.15×10^{-2}	1.04×10^{-1}	1.15×10^{-1}	1.26×10^{-50}	9.84×10^{-50}
#	T_C (GeV)	T_N (GeV)	α	β/H_*	$(\Omega_{\rm GW} h^2)_{\rm max}$
1	277.5	144.6	0.22	796.068	5.26×10^{-12}
2	416.5	210.2	0.09	996.56	2.08×10^{-13}
3	456	214.7	0.05	1501.05	1.53×10^{-14}

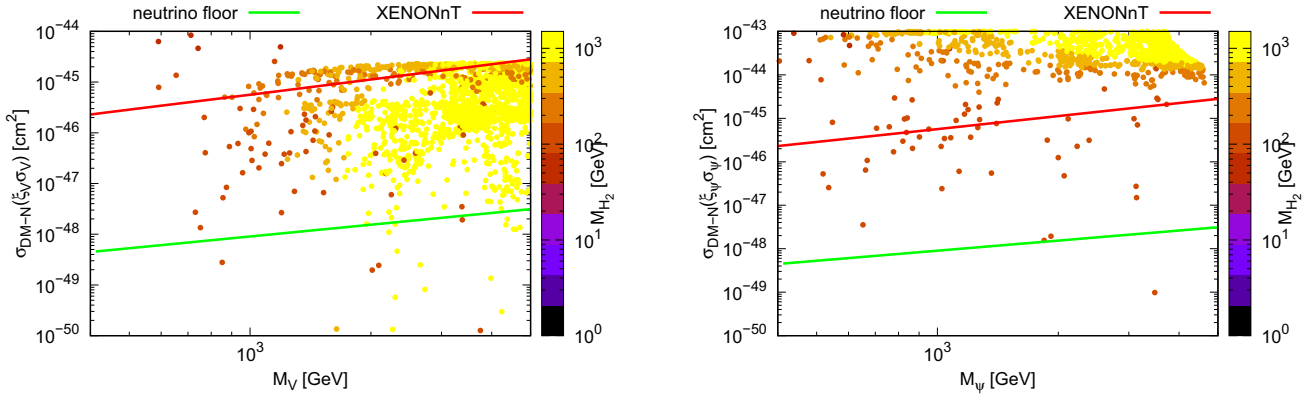

Fig. 9 The allowed range of parameter space consistent with DM relic density and DD. In **a** $\xi_V \sigma_V$ VS M_V and in **b** $\xi_\psi \sigma_\psi$ VS M_ψ has shown

where

$$\mu_{VN} = M_N M_V/(M_N+M_V),\ \mu_\psi = M_N M_\psi/(M_N+M_\psi). \tag{4.11}$$

M_N is the nucleon mass and $f_N \simeq 0.3$ parameterizes the Higgs-nucleon coupling.

Various DD experiments have placed constraints on DM-Nucleon spin independent cross section, such as LUX [120], PandaX-II [121], XENON1T [122], LZ [123] and XENONnT [98]. Of course, these experiments are gradually approaching what is called the neutrino floor [124], which is a the irreducible background coming from scattering of SM neutrinos on nucleons. We use the XENONnT [98] experiment results to constrain the parameter space of our model. In this experiment there is a minimum upper limit on the spin-independent WIMP-nucleon cross section of 2.58×10^{-47} cm^2 for a WIMP mass of 28 GeV. In order to study the effect of the direct detection experiment on the model, we use rescaled DM-Nucleon cross section $\xi_V \sigma_V$ and $\xi_\psi \sigma_\psi$.

In Fig. 9, rescaled DM-Nucleon cross sections($\xi_V \sigma_V$ and $\xi_\psi \sigma_\psi$) are depicted for the parameters that are in agreement with the relic density. It is clear from the figure that there are some points between the XENONnT direct detection bound and the neutrino floor which can be probed in future direct detection experiments. As is expected from 4.10, by reducing the mass difference between H_1 and H_2, the cross section decreases and therefore allowable points increase. In our model, DM interacts with nucleons through H_1 and H_2 mediators. The relevant terms in the Lagrangian are $Ah_1[\bar{q}q]$ and $Bh_2[V_\mu V^\mu\ (\bar{\psi}\psi)]$ for vector (spinor) DM, where A and B are some constants. Therefore, the H_1 mediator involves $A\cos\alpha H_1[\bar{q}q] - B\sin\alpha H_1[V_\mu V^\mu\ (\bar{\psi}\psi)]$. Similarly, for the H_2 mediator, the terms are $A\sin\alpha H_2[\bar{q}q] + B\cos\alpha H_2[V_\mu V^\mu\ (\bar{\psi}\psi)]$. Consequently, the effective 5(6)-dimensional interaction terms for DM-quark interactions at low energies will be $AB\sin\alpha\cos\alpha\left(\frac{1}{M_{H_2}^2} - \frac{1}{M_{H_1}^2}\right)[\bar{q}q][V_\mu V^\mu\ (\bar{\psi}\psi)]$. Around

$M_{H_2} \simeq M_{H_1}$, the effective coupling between DM and quarks approaches zero, resulting in a dip in the DM-nucleon cross-section. In [125], a study has been done on degenerate Higgs scenario. In [126], it is shown by using the high resolution of the diphoton channel of the Higgs boson decays, that the mass difference between the two degenerate states $\Delta m \gtrsim 3$ GeV is disfavored at the 2σ level from the LHC Run-I data. In order to test a degenerate Higgs scenario, a possible proposal is consideration of degenerate scalar productions at the International Linear Collider (ILC) [127]. It was shown [125] that for $\Delta m \gtrsim 1$ GeV, it is possible to distinguish between two Higgs.

4.1.3 Invisible Higgs decay

In this scenario, according to Fig. 9, because there is no point where $M_{\psi,V,H_2} < M_{H1}/2$, it is not necessary to check the invisible Higgs decay.

4.2 Electroweak phase transition and gravitational waves

To investigate the phase transition and the resulting GWs, we follow the procedure of Sect. 3.2. We select three benchmark points as shown in Table 3. Benchmarks 1 and 2 are consistent with direct detection constraint, while benchmark 3 is placed under the neutrino floor. Figure 10 shows the changes of potential and S_3/T in terms of temperature. The GW spec-

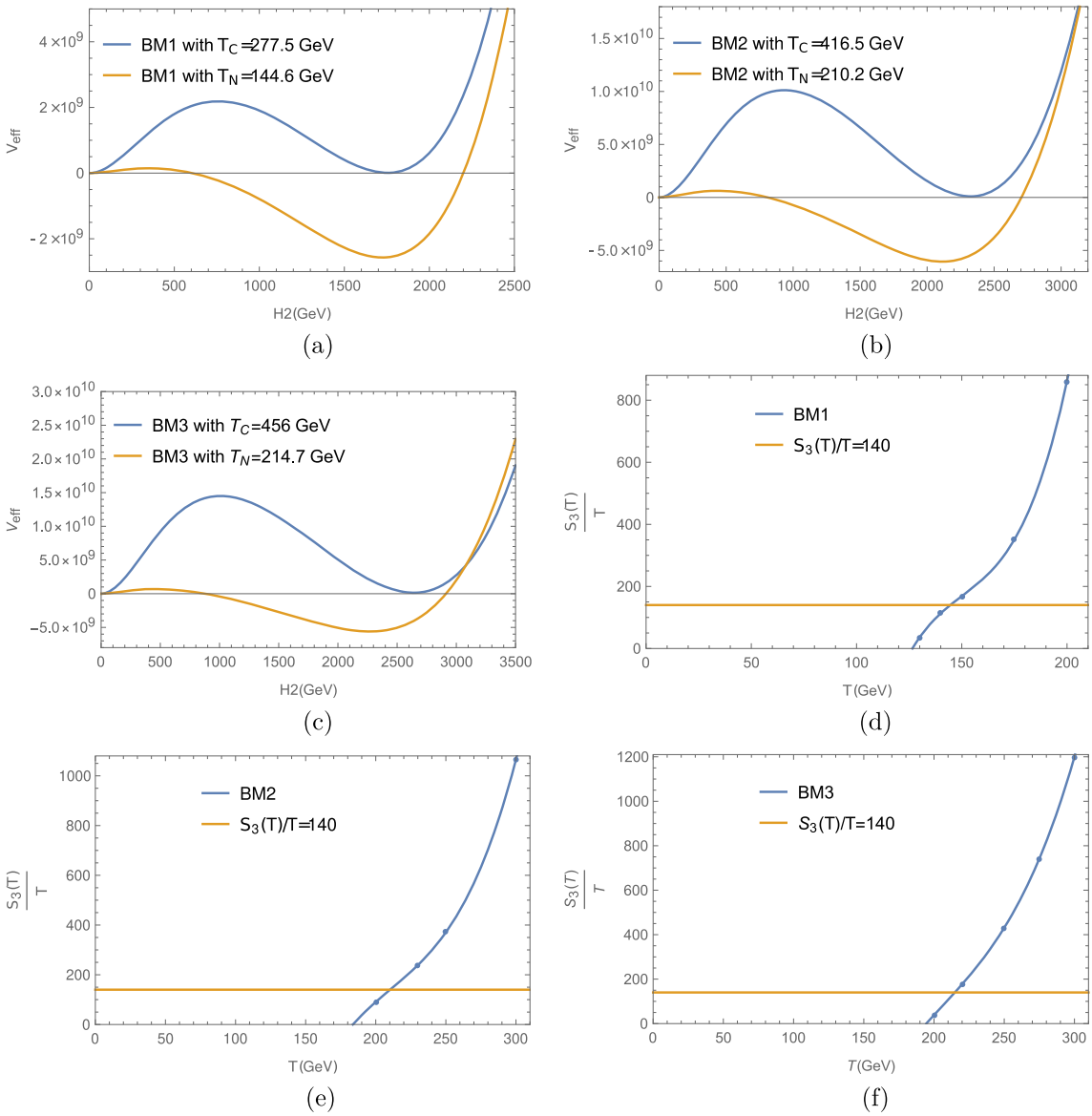

Fig. 10 In **a**, **b** and **c** Potential behavior are given for critical temperature and nucleation temperature. In **d**, **e** and **f** S_3/T changes in terms of temperature are also given for all three benchmarks

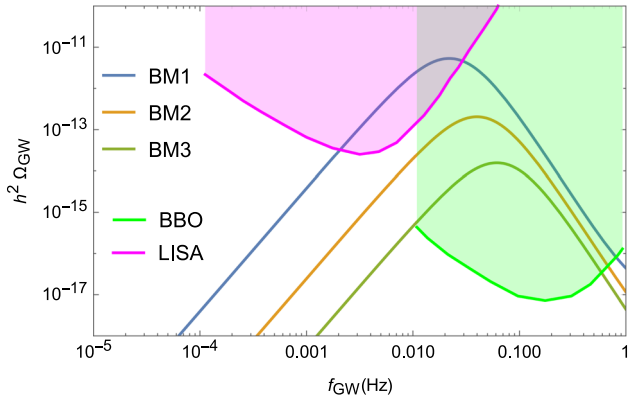

Fig. 11 GW spectrum for benchmark points of the Table 3

trum for these benchmark points is depicted in Fig. 11. The GW spectrum for these benchmarks falls within the observational window of BBO. For benchmark 1, the gravitational wave peak will also be in LISA's range. For the benchmark 3, which is below the neutrino floor limit, future gravitational wave detectors can provide a special way to discover and investigate this area.

5 Conclusion

We have considered an extension of the SM with a new $U(1)$ symmetry in the dark part. According to the new particle mass in the model, we considered two different scenarios. The model consists of three new fields: a fermion, a complex scalar, and a vector field. In scenario A, only fermionic particles are considered as DM. In scenario B, both vector and fermionic particles are considered as DM. The model has classical scale symmetry; electroweak symmetry breaking occurs through Gildener–Weinberg mechanism and gives a natural solution to the hierarchy problem. Numerical solution of the Boltzmann equations for both scenarios was conducted to determine a parameter space region which is compatible with Planck and XENONnT data and collider constraints (invisible Higgs decay in scenario A). A three-dimensional parameter space acquisition was completed.

We focused our attention on the phase transition dynamics after presenting the model and exploring DM phenomenology. The full finite-temperature effective potential of the model at the one-loop level was obtained to investigate the nature and strength of the electroweak phase transition, with the aim of exploring its nature and strength. A first-order electroweak phase transition can exist when there is a barrier between the broken and symmetric phases. It was demonstrated that the finite-temperature effects induce such a barrier and thereby give rise to a phase transition which can generate GWs.

After studying the phase transition, we investigated the resulting GWs. The parameters required to investigate GWs can all be calculated from our presented model and are a function of the independent parameters of the model. We have demonstrated that the model can survive DM relic density, direct detection and collider constraints, while also producing GWs during the first-order electroweak phase transition. We also showed that GWs can be a special probe for the benchmarks that are placed under the neutrino floor (benchmark 3 in both scenarios). These waves can be placed within the observation window of LISA and BBO, which is hoped to be a path to new physics.

Data Availability Statement This manuscript has no associated data or the data will not be deposited. [Authors' comment: Experimental Datasets derived from public resources and other data that support the findings of this study are available on request from the corresponding author.]

Code Availability Statement Code/software will be made available on reasonable request. [Authors' comment: Codes used in this paper are available on request from the corresponding author.]

Funded by SCOAP[3].

References

1. G. Bertone, D. Hooper, History of dark matter. Rev. Mod. Phys. **90**, 045002 (2018). https://doi.org/10.1103/RevModPhys.90.045002. arXiv:1605.04909
2. J.L. Feng, The WIMP paradigm: theme and variations, in *Les Houches summer school on Dark Matter*, p. 12 (2022). https://doi.org/10.21468/SciPostPhysLectNotes.71. arXiv:2212.02479
3. K.M. Zurek, Multi-component dark matter. Phys. Rev. D **79**, 115002 (2009). https://doi.org/10.1103/PhysRevD.79.115002. arXiv:0811.4429
4. S. Profumo, K. Sigurdson, L. Ubaldi, Can we discover multi-component WIMP dark matter? JCAP **12**, 016 (2009). https://doi.org/10.1088/1475-7516/2009/12/016. arXiv:0907.4374
5. M. Aoki, M. Duerr, J. Kubo, H. Takano, Multi-component dark matter systems and their observation prospects. Phys. Rev. D **86**, 076015 (2012). https://doi.org/10.1103/PhysRevD.86.076015. arXiv:1207.3318
6. A. Biswas, D. Majumdar, A. Sil, P. Bhattacharjee, Two component dark matter?: a possible explanation of 130 GeV γ-ray line from the Galactic Centre. JCAP **12**, 049 (2013). https://doi.org/10.1088/1475-7516/2013/12/049. arXiv:1301.3668
7. P.-H. Gu, Multi-component dark matter with magnetic moments for Fermi-LAT gamma-ray line. Phys. Dark Univ. **2**, 35 (2013). https://doi.org/10.1016/j.dark.2013.03.001. arXiv:1301.4368

8. M. Aoki, J. Kubo, H. Takano, Two-loop radiative seesaw mechanism with multicomponent dark matter explaining the possible γ excess in the Higgs boson decay and at the Fermi LAT. Phys. Rev. D **87**, 116001 (2013). https://doi.org/10.1103/PhysRevD.87.116001. arXiv:1302.3936
9. Y. Kajiyama, H. Okada, T. Toma, Multicomponent dark matter particles in a two-loop neutrino model. Phys. Rev. D **88**, 015029 (2013). https://doi.org/10.1103/PhysRevD.88.015029. arXiv:1303.7356
10. L. Bian, R. Ding, B. Zhu, Two component Higgs-portal dark matter. Phys. Lett. B **728**, 105 (2014). https://doi.org/10.1016/j.physletb.2013.11.034. arXiv:1308.3851
11. S. Bhattacharya, A. Drozd, B. Grzadkowski, J. Wudka, Two-component dark matter. JHEP **10**, 158 (2013). https://doi.org/10.1007/JHEP10(2013)158. arXiv:1309.2986
12. C.-Q. Geng, D. Huang, L.-H. Tsai, Imprint of multicomponent dark matter on AMS-02. Phys. Rev. D **89**, 055021 (2014). https://doi.org/10.1103/PhysRevD.89.055021. arXiv:1312.0366
13. S. Esch, M. Klasen, C.E. Yaguna, A minimal model for two-component dark matter. JHEP **09**, 108 (2014). https://doi.org/10.1007/JHEP09(2014)108. arXiv:1406.0617
14. K.R. Dienes, J. Kumar, B. Thomas, D. Yaylali, Dark-matter decay as a complementary probe of multicomponent dark sectors. Phys. Rev. Lett. **114**, 051301 (2015). https://doi.org/10.1103/PhysRevLett.114.051301. arXiv:1406.4868
15. L. Bian, T. Li, J. Shu, X.-C. Wang, Two component dark matter with multi-Higgs portals. JHEP **03**, 126 (2015). https://doi.org/10.1007/JHEP03(2015)126. arXiv:1412.5443
16. C.-Q. Geng, D. Huang, C. Lai, Revisiting multicomponent dark matter with new AMS-02 data. Phys. Rev. D **91**, 095006 (2015). https://doi.org/10.1103/PhysRevD.91.095006. arXiv:1411.4450
17. A. DiFranzo, G. Mohlabeng, Multi-component dark matter through a radiative Higgs portal. JHEP **01**, 080 (2017). https://doi.org/10.1007/JHEP01(2017)080. arXiv:1610.07606
18. M. Aoki, T. Toma, Implications of two-component dark matter induced by forbidden channels and thermal freeze-out. JCAP **01**, 042 (2017). https://doi.org/10.1088/1475-7516/2017/01/042. arXiv:1611.06746
19. A. Dutta Banik, M. Pandey, D. Majumdar, A. Biswas, Two component WIMP-FImP dark matter model with singlet fermion, scalar and pseudo scalar. Eur. Phys. J. C **77**, 657 (2017). https://doi.org/10.1140/epjc/s10052-017-5221-y. arXiv:1612.08621
20. M. Pandey, D. Majumdar, K.P. Modak, Two component feebly interacting massive particle (FIMP) dark matter. JCAP **06**, 023 (2018). https://doi.org/10.1088/1475-7516/2018/06/023. arXiv:1709.05955
21. D. Borah, A. Dasgupta, U.K. Dey, S. Patra, G. Tomar, Multi-component fermionic dark matter and IceCube PeV scale neutrinos in left-right model with gauge unification. JHEP **09**, 005 (2017). https://doi.org/10.1007/JHEP09(2017)005. arXiv:1704.04138
22. J. Herrero-Garcia, A. Scaffidi, M. White, A.G. Williams, On the direct detection of multi-component dark matter: sensitivity studies and parameter estimation. JCAP **11**, 021 (2017). https://doi.org/10.1088/1475-7516/2017/11/021. arXiv:1709.01945
23. A. Ahmed, M. Duch, B. Grzadkowski, M. Iglicki, Multi-component dark matter: the vector and fermion case. Eur. Phys. J. C **78**, 905 (2018). https://doi.org/10.1140/epjc/s10052-018-6371-2. arXiv:1710.01853
24. S. Peyman Zakeri, S. Mohammad Moosavi Nejad, M. Zakeri, S. Ayazi, A minimal model for two-component FIMP dark matter: a basic search. Chin. Phys. C **42**, 073101 (2018). https://doi.org/10.1088/1674-1137/42/7/073101. arXiv:1801.09115
25. M. Aoki, T. Toma, Boosted self-interacting dark matter in a multi-component dark matter model. JCAP **10**, 020 (2018). https://doi.org/10.1088/1475-7516/2018/10/020. arXiv:1806.09154
26. S. Chakraborti, P. Poulose, Interplay of scalar and fermionic components in a multi-component dark matter scenario. Eur. Phys. J. C **79**, 420 (2019). https://doi.org/10.1140/epjc/s10052-019-6933-y. arXiv:1808.01979
27. N. Bernal, D. Restrepo, C. Yaguna, O. Zapata, Two-component dark matter and a massless neutrino in a new $B-L$ model. Phys. Rev. D **99**, 015038 (2019). https://doi.org/10.1103/PhysRevD.99.015038. arXiv:1808.03352
28. A. Poulin, S. Godfrey, Multicomponent dark matter from a hidden gauged SU(3). Phys. Rev. D **99**, 076008 (2019). https://doi.org/10.1103/PhysRevD.99.076008. arXiv:1808.04901
29. J. Herrero-Garcia, A. Scaffidi, M. White, A.G. Williams, On the direct detection of multi-component dark matter: implications of the relic abundance. JCAP **01**, 008 (2019). https://doi.org/10.1088/1475-7516/2019/01/008. arXiv:1809.06881
30. S. Yaser Ayazi, A. Mohamadnejad, Scale-invariant two component dark matter. Eur. Phys. J. C **79**, 140 (2019). https://doi.org/10.1140/epjc/s10052-019-6651-5. arXiv:1808.08706
31. F. Elahi, S. Khatibi, Multi-component dark matter in a non-abelian dark sector. Phys. Rev. D **100**, 015019 (2019). https://doi.org/10.1103/PhysRevD.100.015019. arXiv:1902.04384
32. D. Borah, A. Dasgupta, S.K. Kang, Two-component dark matter with cogenesis of the baryon asymmetry of the Universe. Phys. Rev. D **100**, 103502 (2019). https://doi.org/10.1103/PhysRevD.100.103502. arXiv:1903.10516
33. S. Bhattacharya, P. Ghosh, A.K. Saha, A. Sil, Two component dark matter with inert Higgs doublet: neutrino mass, high scale validity and collider searches. JHEP **03**, 090 (2020). https://doi.org/10.1007/JHEP03(2020)090. arXiv:1905.12583
34. A. Biswas, D. Borah, D. Nanda, Type III seesaw for neutrino masses in $U(1)_{BL}$ model with multi-component dark matter. JHEP **12**, 109 (2019). https://doi.org/10.1007/JHEP12(2019)109. arXiv:1908.04308
35. D. Nanda, D. Borah, Connecting light dirac neutrinos to a multi-component dark matter scenario in gauged $B-L$ model. Eur. Phys. J. C **80**, 557 (2020). https://doi.org/10.1140/epjc/s10052-020-8122-4. arXiv:1911.04703
36. C.E. Yaguna, O. Zapata, Multi-component scalar dark matter from a Z_N symmetry: a systematic analysis. JHEP **03**, 109 (2020). https://doi.org/10.1007/JHEP03(2020)109. arXiv:1911.05515
37. G. Bélanger, A. Pukhov, C.E. Yaguna, O. Zapata, The Z_5 model of two-component dark matter. JHEP **09**, 030 (2020). https://doi.org/10.1007/JHEP09(2020)030. arXiv:2006.14922
38. P. Van Dong, C.H. Nam, D. Van Loi, Canonical seesaw implication for two-component dark matter. Phys. Rev. D **103**, 095016 (2021). https://doi.org/10.1103/PhysRevD.103.095016. arXiv:2007.08957
39. S. Khalil, S. Moretti, D. Rojas-Ciofalo, H. Waltari, Multicomponent dark matter in a simplified E_6SSM. Phys. Rev. D **102**, 075039 (2020). https://doi.org/10.1103/PhysRevD.102.075039. arXiv:2007.10966
40. A. Dutta Banik, R. Roshan, A. Sil, Two component singlet-triplet scalar dark matter and electroweak vacuum stability. Phys. Rev. D **103**, 075001 (2021). https://doi.org/10.1103/PhysRevD.103.075001. arXiv:2009.01262
41. J. Hernandez-Sanchez, V. Keus, S. Moretti, D. Rojas-Ciofalo, D. Sokolowska, Complementary probes of two-component dark matter. arXiv:2012.11621
42. N. Chakrabarty, R. Roshan, A. Sil, Two-component doublet-triplet scalar dark matter stabilizing the electroweak vacuum. Phys. Rev. D **105**, 115010 (2022). https://doi.org/10.1103/PhysRevD.105.115010. arXiv:2102.06032
43. C.E. Yaguna, O. Zapata, Two-component scalar dark matter in Z_{2n} scenarios. JHEP **10**, 185 (2021). https://doi.org/10.1007/JHEP10(2021)185. arXiv:2106.11889

44. B. Díaz Sáez, P. Escalona, S. Norero, A.R. Zerwekh, Fermion singlet dark matter in a pseudoscalar dark matter portal. JHEP **10**, 233 (2021). https://doi.org/10.1007/JHEP10(2021)233. arXiv:2105.04255
45. B. Díaz Sáez, K. Möhling, D. Stöckinger, Two real scalar WIMP model in the assisted freeze-out scenario. JCAP **10**, 027 (2021). https://doi.org/10.1088/1475-7516/2021/10/027. arXiv:2103.17064
46. Y.G. Kim, K.Y. Lee, S.-H. Nam, Phenomenology of a two-component dark matter model. Phys. Lett. B **834**, 137412 (2022). https://doi.org/10.1016/j.physletb.2022.137412. arXiv:2201.11485
47. S.-Y. Ho, P. Ko, C.-T. Lu, Scalar and fermion two-component SIMP dark matter with an accidental $\mathbb{Z}_4$ symmetry. JHEP **03**, 005 (2022). https://doi.org/10.1007/JHEP03(2022)005. arXiv:2201.06856
48. F. Costa, S. Khan, J. Kim, A two-component dark matter model and its associated gravitational waves. JHEP **06**, 026 (2022). https://doi.org/10.1007/JHEP06(2022)026. arXiv:2202.13126
49. S. Bhattacharya, P. Ghosh, J. Lahiri, B. Mukhopadhyaya, Mono-X signal and two component dark matter: new distinction criteria. arXiv:2211.10749
50. S. Bhattacharya, P. Ghosh, J. Lahiri, B. Mukhopadhyaya, Distinguishing two dark matter component particles at e^+e colliders. JHEP **12**, 049 (2022). https://doi.org/10.1007/JHEP12(2022)049. arXiv:2202.12097
51. S. Bhattacharya, P. Ghosh, N. Sahu, Multipartite dark matter with scalars, fermions and signatures at LHC. JHEP **02**, 059 (2019). https://doi.org/10.1007/JHEP02(2019)059. arXiv:1809.07474
52. S. Bhattacharya, P. Poulose, P. Ghosh, Multipartite interacting scalar dark matter in the light of updated LUX data. JCAP **04**, 043 (2017). https://doi.org/10.1088/1475-7516/2017/04/043. arXiv:1607.08461
53. A. Mohamadnejad, Electroweak phase transition and gravitational waves in a two-component dark matter model. JHEP **03**, 188 (2022). https://doi.org/10.1007/JHEP03(2022)188. arXiv:2111.04342
54. K. Kajantie, M. Laine, K. Rummukainen, M.E. Shaposhnikov, Is there a hot electroweak phase transition at $m_H \gtrsim m_W$? Phys. Rev. Lett. **77**, 2887 (1996). https://doi.org/10.1103/PhysRevLett.77.2887. arXiv:hep-ph/9605288
55. Y. Aoki, F. Csikor, Z. Fodor, A. Ukawa, The endpoint of the first order phase transition of the SU(2) gauge Higgs model on a four-dimensional isotropic lattice. Phys. Rev. D **60**, 013001 (1999). https://doi.org/10.1103/PhysRevD.60.013001. arXiv:hep-lat/9901021
56. D.J. Weir, Gravitational waves from a first order electroweak phase transition: a brief review. Philos. Trans. R. Soc. Lond. A **376**, 20170126 (2018). https://doi.org/10.1098/rsta.2017.0126. arXiv:1705.01783
57. M. Chala, G. Nardini, I. Sobolev, Unified explanation for dark matter and electroweak baryogenesis with direct detection and gravitational wave signatures. Phys. Rev. D **94**, 055006 (2016). https://doi.org/10.1103/PhysRevD.94.055006. arXiv:1605.08663
58. A. Soni, Y. Zhang, Gravitational waves from SU(N) glueball dark matter. Phys. Lett. B **771**, 379 (2017). https://doi.org/10.1016/j.physletb.2017.05.077. arXiv:1610.06931
59. R. Flauger, S. Weinberg, Gravitational waves in cold dark matter. Phys. Rev. D **97**, 123506 (2018). https://doi.org/10.1103/PhysRevD.97.123506. arXiv:1801.00386
60. I. Baldes, Gravitational waves from the asymmetric-dark-matter generating phase transition. JCAP **05**, 028 (2017). https://doi.org/10.1088/1475-7516/2017/05/028. arXiv:1702.02117
61. W. Chao, H.-K. Guo, J. Shu, Gravitational wave signals of electroweak phase transition triggered by dark matter. JCAP **09**, 009 (2017). https://doi.org/10.1088/1475-7516/2017/09/009. arXiv:1702.02698
62. A. Beniwal, M. Lewicki, J.D. Wells, M. White, A.G. Williams, Gravitational wave, collider and dark matter signals from a scalar singlet electroweak baryogenesis. JHEP **08**, 108 (2017). https://doi.org/10.1007/JHEP08(2017)108. arXiv:1702.06124
63. F.P. Huang, J.-H. Yu, Exploring inert dark matter blind spots with gravitational wave signatures. Phys. Rev. D **98**, 095022 (2018). https://doi.org/10.1103/PhysRevD.98.095022. arXiv:1704.04201
64. F.P. Huang, C.S. Li, Probing the baryogenesis and dark matter relaxed in phase transition by gravitational waves and colliders. Phys. Rev. D **96**, 095028 (2017). https://doi.org/10.1103/PhysRevD.96.095028. arXiv:1709.09691
65. E. Madge, P. Schwaller, Leptophilic dark matter from gauged lepton number: phenomenology and gravitational wave signatures. JHEP **02**, 048 (2019). https://doi.org/10.1007/JHEP02(2019)048. arXiv:1809.09110
66. L. Bian, Y.-L. Tang, Thermally modified sterile neutrino portal dark matter and gravitational waves from phase transition: the freeze-in case. JHEP **12**, 006 (2018). https://doi.org/10.1007/JHEP12(2018)006. arXiv:1810.03172
67. L. Bian, X. Liu, Two-step strongly first-order electroweak phase transition modified FIMP dark matter, gravitational wave signals, and the neutrino mass. Phys. Rev. D **99**, 055003 (2019). https://doi.org/10.1103/PhysRevD.99.055003. arXiv:1811.03279
68. V.R. Shajiee, A. Tofighi, Electroweak phase transition, gravitational waves and dark matter in two scalar singlet extension of the standard model. Eur. Phys. J. C **79**, 360 (2019). https://doi.org/10.1140/epjc/s10052-019-6881-6. arXiv:1811.09807
69. K. Kannike, M. Raidal, Phase transitions and gravitational wave tests of pseudo-goldstone dark matter in the softly broken U(1) scalar singlet model. Phys. Rev. D **99**, 115010 (2019). https://doi.org/10.1103/PhysRevD.99.115010. arXiv:1901.03333
70. S. Yaser Ayazi, A. Mohamadnejad, Conformal vector dark matter and strongly first-order electroweak phase transition. JHEP **03**, 181 (2019). https://doi.org/10.1007/JHEP03(2019)181. arXiv:1901.04168
71. A. Mohamadnejad, Gravitational waves from scale-invariant vector dark matter model: probing below the neutrino-floor. Eur. Phys. J. C **80**, 197 (2020). https://doi.org/10.1140/epjc/s10052-020-7756-6. arXiv:1907.08899
72. K. Kannike, K. Loos, M. Raidal, Gravitational wave signals of pseudo-Goldstone dark matter in the $\mathbb{Z}_3$ complex singlet model. Phys. Rev. D **101**, 035001 (2020). https://doi.org/10.1103/PhysRevD.101.035001. arXiv:1907.13136
73. A. Paul, B. Banerjee, D. Majumdar, Gravitational wave signatures from an extended inert doublet dark matter model. JCAP **10**, 062 (2019). https://doi.org/10.1088/1475-7516/2019/10/062. arXiv:1908.00829
74. B. Barman, A. Dutta Banik, A. Paul, Singlet-doublet fermionic dark matter and gravitational waves in a two-Higgs-doublet extension of the Standard Model. Phys. Rev. D **101**, 055028 (2020). https://doi.org/10.1103/PhysRevD.101.055028. arXiv:1912.12899
75. D. Marfatia, P.-Y. Tseng, Gravitational wave signals of dark matter freeze-out. JHEP **02**, 022 (2021). https://doi.org/10.1007/JHEP02(2021)022. arXiv:2006.07313
76. T. Alanne, N. Benincasa, M. Heikinheimo, K. Kannike, V. Keus, N. Koivunen et al., Pseudo-Goldstone dark matter: gravitational waves and direct-detection blind spots. JHEP **10**, 080 (2020). https://doi.org/10.1007/JHEP10(2020)080. arXiv:2008.09605
77. X.-F. Han, L. Wang, Y. Zhang, Dark matter, electroweak phase transition, and gravitational waves in the type II two-Higgs-doublet model with a singlet scalar field. Phys. Rev. D **103**,

035012 (2021). https://doi.org/10.1103/PhysRevD.103.035012. arXiv:2010.03730
78. Y. Wang, C.S. Li, F.P. Huang, Complementary probe of dark matter blind spots by lepton colliders and gravitational waves. Phys. Rev. D **104**, 053004 (2021). https://doi.org/10.1103/PhysRevD.104.053004. arXiv:2012.03920
79. X. Deng, X. Liu, J. Yang, R. Zhou, L. Bian, Heavy dark matter and gravitational waves. Phys. Rev. D **103**, 055013 (2021). https://doi.org/10.1103/PhysRevD.103.055013. arXiv:2012.15174
80. W. Chao, X.-F. Li, L. Wang, Filtered pseudo-scalar dark matter and gravitational waves from first order phase transition. JCAP **06**, 038 (2021). https://doi.org/10.1088/1475-7516/2021/06/038. arXiv:2012.15113
81. Z. Zhang, C. Cai, X.-M. Jiang, Y.-L. Tang, Z.-H. Yu, H.-H. Zhang, Phase transition gravitational waves from pseudo-Nambu-Goldstone dark matter and two Higgs doublets. JHEP **05**, 160 (2021). https://doi.org/10.1007/JHEP05(2021)160. arXiv:2102.01588
82. J. Liu, X.-P. Wang, K.-P. Xie, Searching for lepton portal dark matter with colliders and gravitational waves. JHEP **06**, 149 (2021). https://doi.org/10.1007/JHEP06(2021)149. arXiv:2104.06421
83. K. Hashino, M. Kakizaki, S. Kanemura, P. Ko, T. Matsui, Gravitational waves from first order electroweak phase transition in models with the $U(1)_X$ gauge symmetry. JHEP **06**, 088 (2018). https://doi.org/10.1007/JHEP06(2018)088. arXiv:1802.02947
84. P. Athron, C. Balázs, A. Fowlie, L. Morris, L. Wu, Cosmological phase transitions: from perturbative particle physics to gravitational waves. arXiv:2305.02357
85. V.V. Khoze, D.L. Milne, Gravitational waves and dark matter from classical scale invariance. Phys. Rev. D **107**, 095012 (2023). https://doi.org/10.1103/PhysRevD.107.095012. arXiv:2212.04784
86. E. Witten, Cosmological consequences of a light Higgs boson. Nucl. Phys. B **177**, 477 (1981). https://doi.org/10.1016/0550-3213(81)90182-6
87. A.H. Guth, E.J. Weinberg, Cosmological consequences of a first order phase transition in the SU(5) grand unified model. Phys. Rev. D **23**, 876 (1981). https://doi.org/10.1103/PhysRevD.23.876
88. P.J. Steinhardt, The Weinberg–Salam model and early cosmology. Nucl. Phys. B **179**, 492 (1981). https://doi.org/10.1016/0550-3213(81)90016-X
89. P.J. Steinhardt, Relativistic detonation waves and bubble growth in false vacuum decay. Phys. Rev. D **25**, 2074 (1982). https://doi.org/10.1103/PhysRevD.25.2074
90. E. Witten, Cosmic separation of phases. Phys. Rev. D **30**, 272 (1984). https://doi.org/10.1103/PhysRevD.30.272
91. LIGO Scientific, Virgo collaboration, Observation of gravitational waves from a binary black hole merger. Phys. Rev. Lett. **116**, 061102 (2016). https://doi.org/10.1103/PhysRevLett.116.061102. arXiv:1602.03837
92. C. Caprini et al., Detecting gravitational waves from cosmological phase transitions with LISA: an update. JCAP **03**, 024 (2020). https://doi.org/10.1088/1475-7516/2020/03/024. arXiv:1910.13125
93. LISA collaboration, Laser Interferometer Space Antenna. arXiv:1702.00786
94. J. Crowder, N.J. Cornish, Beyond LISA: exploring future gravitational wave missions. Phys. Rev. D **72**, 083005 (2005). https://doi.org/10.1103/PhysRevD.72.083005. arXiv:gr-qc/0506015
95. M.E. Shaposhnikov, Baryon asymmetry of the universe in standard electroweak theory. Nucl. Phys. B **287**, 757 (1987). https://doi.org/10.1016/0550-3213(87)90127-1
96. S.R. Coleman, E.J. Weinberg, Radiative corrections as the origin of spontaneous symmetry breaking. Phys. Rev. D **7**, 1888 (1973). https://doi.org/10.1103/PhysRevD.7.1888
97. Planck collaboration, Planck 2018 results. VI. Cosmological parameters. Astron. Astrophys. **641**, A6 (2020). https://doi.org/10.1051/0004-6361/201833910. arXiv:1807.06209
98. XENON collaboration, First Dark Matter Search with Nuclear Recoils from the XENONnT Experiment. arXiv:2303.14729
99. E. Gildener, S. Weinberg, Symmetry breaking and scalar bosons. Phys. Rev. D **13**, 3333 (1976). https://doi.org/10.1103/PhysRevD.13.3333
100. D. Barducci, G. Belanger, J. Bernon, F. Boudjema, J. Da Silva, S. Kraml et al., Collider limits on new physics within micrOMEGAs_4.3. Comput. Phys. Commun. **222**, 327 (2018). https://doi.org/10.1016/j.cpc.2017.08.028. arXiv:1606.03834
101. LHC Higgs Cross Section Working Group collaboration, Handbook of LHC Higgs Cross Sections: 1. Inclusive Observables. arXiv:1101.0593
102. A. Denner, S. Heinemeyer, I. Puljak, D. Rebuzzi, M. Spira, Standard model Higgs-boson branching ratios with uncertainties. Eur. Phys. J. C **71**, 1753 (2011). https://doi.org/10.1140/epjc/s10052-011-1753-8. arXiv:1107.5909
103. S. Dittmaier et al., Handbook of LHC Higgs Cross Sections: 2. Differential Distributions. arXiv:1201.3084
104. O. Brein, A. Djouadi, R. Harlander, NNLO QCD corrections to the Higgs–Strahlung processes at hadron colliders. Phys. Lett. B **579**, 149 (2004). https://doi.org/10.1016/j.physletb.2003.10.112. arXiv:hep-ph/0307206
105. LHC Higgs Cross Section Working Group collaboration, Handbook of LHC Higgs Cross Sections: 3. Higgs Properties. arXiv:1307.1347
106. CMS collaboration, Search for invisible decays of the Higgs boson produced via vector boson fusion in proton-proton collisions at s=13 TeV. Phys. Rev. D **105**, 092007 (2022). https://doi.org/10.1103/PhysRevD.105.092007. arXiv:2201.11585
107. ATLAS collaboration, Search for invisible Higgs-boson decays in events with vector-boson fusion signatures using 139 fb^{-1} of proton-proton data recorded by the ATLAS experiment. JHEP **08**, 104 (2022). https://doi.org/10.1007/JHEP08(2022)104. arXiv:2202.07953
108. L. Dolan, R. Jackiw, Symmetry behavior at finite temperature. Phys. Rev. D **9**, 3320 (1974). https://doi.org/10.1103/PhysRevD.9.3320
109. M.E. Carrington, The effective potential at finite temperature in the standard model. Phys. Rev. D **45**, 2933 (1992). https://doi.org/10.1103/PhysRevD.45.2933
110. M.E. Shaposhnikov, Possible appearance of the baryon asymmetry of the universe in an electroweak theory. JETP Lett. **44**, 465 (1986)
111. R. Apreda, M. Maggiore, A. Nicolis, A. Riotto, Gravitational waves from electroweak phase transitions. Nucl. Phys. B **631**, 342 (2002). https://doi.org/10.1016/S0550-3213(02)00264-X. arXiv:gr-qc/0107033
112. A. Masoumi, K.D. Olum, J.M. Wachter, Approximating tunneling rates in multi-dimensional field spaces. JCAP **10**, 022 (2017). https://doi.org/10.1088/1475-7516/2017/10/022. arXiv:1702.00356
113. D. Bodeker, G.D. Moore, Can electroweak bubble walls run away? JCAP **05**, 009 (2009). https://doi.org/10.1088/1475-7516/2009/05/009. arXiv:0903.4099
114. S.J. Huber, T. Konstandin, Gravitational wave production by collisions: more bubbles. JCAP **09**, 022 (2008). https://doi.org/10.1088/1475-7516/2008/09/022. arXiv:0806.1828
115. M. Hindmarsh, S.J. Huber, K. Rummukainen, D.J. Weir, Numerical simulations of acoustically generated gravitational waves at a first order phase transition. Phys. Rev. D **92**, 123009 (2015). https://doi.org/10.1103/PhysRevD.92.123009. arXiv:1504.03291

116. C. Caprini, R. Durrer, G. Servant, The stochastic gravitational wave background from turbulence and magnetic fields generated by a first-order phase transition. JCAP **12**, 024 (2009). https://doi.org/10.1088/1475-7516/2009/12/024. arXiv:0909.0622
117. C. Caprini et al., Science with the space-based interferometer eLISA. II: gravitational waves from cosmological phase transitions. JCAP **04**, 001 (2016). https://doi.org/10.1088/1475-7516/2016/04/001. arXiv:1512.06239
118. M. Kamionkowski, A. Kosowsky, M.S. Turner, Gravitational radiation from first order phase transitions. Phys. Rev. D **49**, 2837 (1994). https://doi.org/10.1103/PhysRevD.49.2837. arXiv:astro-ph/9310044
119. G. Bélanger, F. Boudjema, A. Pukhov, A. Semenov, micrOMEGAs4.1: two dark matter candidates. Comput. Phys. Commun. **192**, 322 (2015). https://doi.org/10.1016/j.cpc.2015.03.003. arXiv:1407.6129
120. LUX collaboration, Results from a search for dark matter in the complete LUX exposure. Phys. Rev. Lett. **118**, 021303 (2017). https://doi.org/10.1103/PhysRevLett.118.021303. arXiv:1608.07648
121. PandaX- II collaboration, Dark matter results from first 98.7 days of data from the PandaX-II Experiment. Phys. Rev. Lett. **117**, 121303 (2016). https://doi.org/10.1103/PhysRevLett.117.121303. arXiv:1607.07400
122. XENON collaboration, Dark matter search results from a one ton-year exposure of XENON1T. Phys. Rev. Lett. **121**, 111302 (2018). https://doi.org/10.1103/PhysRevLett.121.111302. arXiv:1805.12562
123. LZ collaboration, First Dark Matter Search Results from the LUX-ZEPLIN (LZ) Experiment. arXiv:2207.03764
124. J. Billard, L. Strigari, E. Figueroa-Feliciano, Implication of neutrino backgrounds on the reach of next generation dark matter direct detection experiments. Phys. Rev. D **89**, 023524 (2014). https://doi.org/10.1103/PhysRevD.89.023524. arXiv:1307.5458
125. S. Abe, G.-C. Cho, K. Mawatari, Probing a degenerate-scalar scenario in a pseudoscalar dark-matter model. Phys. Rev. D **104**, 035023 (2021). https://doi.org/10.1103/PhysRevD.104.035023. [arXiv:2101.04887]
126. CMS collaboration, Observation of the diphoton decay of the Higgs boson and measurement of its properties. Eur. Phys. J. C **74**, 3076 (2014). https://doi.org/10.1140/epjc/s10052-014-3076-z. arXiv:1407.0558
127. The International Linear Collider Technical Design Report—Volume 1: Executive Summary. arXiv:1306.6327